Light-nuclei production in heavy-ion collisions within a thermodynamical approach

M. Kozhevnikova [1,*] and Yu. B. Ivanov [2,3,4,†]

[1] *Veksler and Baldin Laboratory of High Energy Physics, JINR Dubna, 141980 Dubna, Russia*

[2] *Bogoliubov Laboratory of Theoretical Physics, JINR Dubna, 141980 Dubna, Russia*

[3] *National Research Nuclear University "MEPhI", 115409 Moscow, Russia*

[4] *National Research Centre "Kurchatov Institute", 123182 Moscow, Russia*

(Received 19 October 2022; accepted 24 January 2023; published 3 February 2023)

We present results of simulations of light-nuclei production in relativistic heavy-ion collisions within the updated Three-fluid Hydrodynamics-based Event Simulator Extended by UrQMD (ultrarelativistic quantum molecular dynamics) final State interactions (THESEUS). The simulations were performed for Pb + Pb and Au + Au collisions in the collision energy range of $\sqrt{s_{NN}} = 6.4$–19.6 GeV. The light-nuclei production is treated within the thermodynamical approach on an equal basis with hadrons. The only additional parameter related to the light nuclei is the energy density of late freeze-out that imitates the afterburner stage of the collision because the light nuclei do not participate in the UrQMD evolution. This parameter is fixed from the condition of the best reproduction of the proton transverse-momentum spectrum after the UrQMD afterburner by that at the late freeze-out. The updated THESEUS results in an imperfect but reasonable reproduction of data on bulk observables of the light nuclei, especially their functional dependence on the collision energy and light-nucleus mass. Various ratios, d/p, t/p, t/d, and $N(t) \times N(p)/N^2(d)$, are also considered. The directed flow of light nuclei turns out to be more involved. Apparently, it requires explicit treatment of the afterburner evolution of light nuclei that violates the kinetic equilibrium. Imperfect reproduction of the light-nuclei data leaves room for medium effects in produced light nuclei.

DOI: 10.1103/PhysRevC.107.024903

I. INTRODUCTION

Interest in the light-nuclei production in heavy-ion collisions has been revived in connection with the search for the conjectured critical point in the QCD phase diagram. The STAR experiment has already found possible indications of the existence of the critical point [1]. This observation was based on a predicted [2] peculiar dependence of the scaled kurtosis of net-proton distribution as a function of the collision energy. Besides, an enhanced production of light nuclei close to the critical point with respect to a noncritical scenario is expected [3–5]. This prediction is based on the expectation that the attractive part of nuclear potential becomes dominated by a long-ranged critical mode of QCD. Abundant production of light nuclei may also result from formation of baryon clusters due to spinodal decomposition associated with a mechanically unstable region in the first-order phase transition [6–10]. This spinodal clumping gets enhanced at the critical point, where fluctuations are too slow for the development of equilibrium mixed phase.

At present, there are several three-dimensional (3D) dynamical models which include the coalescence mechanism of the light-nuclei production [11–20]; see also a recent review [21]. In the simplest version, the coalescence-based models deduce the relevant parameters from comparison with data on the light-nuclei production [11,12]. Therefore, their predictive power is restricted. However, the refined coalescence calculations are very successful in reproducing data in a wide range of collision energies [18]. Advanced coalescence approaches involve the Wigner functions of light nuclei [13,14,16,17,19,20] to calculate the coalescence parameters. The recently developed transport models, such as SMASH (simulating many accelerated strongly interacting hadrons) [22–24], PHQMD (parton-hadron quantum molecular dynamics) [25–27], and a stochastic kinetic approach [28], treat light nuclei microscopically (so far, only deuterons in SMASH [23,24]) on an equal basis with other hadrons. However, these transport models also require an extensive additional input for treatment the light-nuclei production, albeit in a wide range of collision energies.

The thermodynamical approach does not need any additional parameters for treatment of the light-nuclei production. It describes the light nuclei in terms of temperatures and chemical potentials, i.e., on an equal basis with hadrons. Therefore, its predictive power is the same for light nuclei and hadrons. This approach was realized within the statistical model [29,30]: deuteron midrapidity yields at the energies (from 7.7 to 200 GeV) of the STAR Beam Energy Scan (BES) at the Relativistic Heavy-Ion Collider (RHIC) [31,32] are described fairly well by this model [33,34], while the yield of tritium is overestimated by roughly a factor of 2 [34,35]. The statistical model gives a similarly good description of not

*kozhevnikova@jinr.ru

†yivanov@theor.jinr.ru

only the light nuclei but even hypernuclei and antinuclei at energies of the CERN Large Hadron Collider (LHC) [36]. The apparent success of the thermal model is puzzling. It is hard to imagine that nuclei exist in the hot and dense fireball environment. The temperature is much higher than the binding energy and the system is quite dense, so that the interparticle spacing is smaller than the typical internucleon distance in a nucleus. This puzzle is discussed in Refs. [4,23,37].

In view of the success of the thermal model, we have implemented the thermodynamic approach for light-nuclei production in the updated THESEUS event generator [38]. In this paper, we address the question of how well this thermodynamic approach can describe the data on the light-nuclei production, provided the bulk observables [39–42] for protons are reasonably well reproduced by the model of three-fluid dynamics (3FD). Note that the model involves no extra parameters (except for the late freeze-out energy density; see Sec. III) related to the light nuclei. For this purpose we analyze the available data from NA49 [43] and STAR [32,35] Collaborations.

II. UPDATED THESEUS

The THESEUS event generator was first presented and its applications to heavy-ion collisions were demonstrated in Refs. [44,45]. THESEUS is based on the 3FD model [12,40] complemented by ultrarelativistic quantum molecular dynamics (UrQMD) [46,47] for the afterburner stage. The output of the 3FD model, i.e., the freeze-out hypersurface, is recorded in terms of local flow velocities and thermodynamic quantities. The THESEUS generator transforms the 3FD output into a set of observed particles, i.e., it performs the particlization.

3FD is designed to simulate heavy-ion collisions at energies of the BES-RHIC at the Brookhaven National Laboratory (BNL), the CERN Super-Proton-Synchrotron (SPS), the Facility for Antiproton and Ion Research (FAIR) in Darmstadt, and the Nuclotron-based Ion Collider fAcility (NICA) in Dubna. It takes into account counterstreaming of the leading baryon-rich matter at the early stage of nuclear collisions. This nonequilibrium stage is modeled by the means of two counterstreaming baryon-rich fluids. Newly produced particles, which dominantly populate the midrapidity region, are assigned to a so-called fireball fluid. These fluids are governed by conventional hydrodynamic equations coupled by friction terms, which describe the energy-momentum exchange between the fluids.

At present, three different equations of state (EoS's) are used in the 3FD simulations: a purely hadronic EoS [48] (hadr. EoS) and two EoS's with deconfinement [49], i.e., an EoS with a first-order phase transition (1PT EoS) and one with a smooth crossover transition (crossover EoS). At energies $\sqrt{s_{NN}} > 5$ GeV, the deconfinement scenarios reveal definite preference [50]. Therefore, in the present work we consider only the 1PT and crossover EoS's.

3FD and the original version of the THESEUS [44,45] calculate spectra of the so-called primordial nucleons, i.e., both observable nucleons and those bound in the light nuclei. This is done for the subsequent application of the coalescence model [12,51] for the light-nuclei production.

TABLE I. Stable light nuclei and low-lying resonances of the ^{4}He system (from BNL properties of nuclides [52]). J denotes the total angular momentum. The last column represents branching ratios of the decay channels, in percent. The p, n, d correspond to the emission of protons, neutrons, or deuterons, respectively.

Nucleus (E [MeV])	J	Decay modes (%)
d	1	Stable
t	1/2	Stable
^{3}He	1/2	Stable
^{4}He	0	Stable
^{4}He(20.21)	0	$p = 100$
^{4}He(21.01)	0	$n = 24$, $p = 76$
^{4}He(21.84)	2	$n = 37$, $p = 63$
^{4}He(23.33)	2	$n = 47$, $p = 53$
^{4}He(23.64)	1	$n = 45$, $p = 55$
^{4}He(24.25)	1	$n = 47$, $p = 50$, $d = 3$
^{4}He(25.28)	0	$n = 48$, $p = 52$
^{4}He(25.95)	1	$n = 48$, $p = 52$
^{4}He(27.42)	2	$n = 3$, $p = 3$, $d = 94$
^{4}He(28.31)	1	$n = 47$, $p = 48$, $d = 5$
^{4}He(28.37)	1	$n = 2$, $p = 2$, $d = 96$
^{4}He(28.39)	2	$n = 0.2$, $p = 0.2$, $d = 99.6$
^{4}He(28.64)	0	$d = 100$
^{4}He(28.67)	2	$d = 100$
^{4}He(29.89)	2	$n = 0.4$, $p = 0.4$, $d = 99.2$

The light nuclei were included in the updated version of the THESEUS [38]. The list of the light nuclei includes stable nuclei and and low-lying resonances of the ^{4}He system, the decays of which contribute to the yields of stable species [3]; see Table I. The corresponding antinuclei were also included. These nuclei are sampled similarly to other hadrons, i.e., according to their phase-space distribution functions. Nevertheless, there is an important difference in the treatment of light nuclei and other hadrons. While the hadrons pass through the UrQMD afterburner stage after the the particlization, the light nuclei do not, just because the UrQMD is not able to treat them. This is a definite shortcoming because the light nuclei are destroyed and reproduced during this afterburner stage [23,24,26].

III. RESULTS

To partially overcome the aforementioned problem of the afterburner stage for the light nuclei, we imitate the afterburner effect by later freeze-out for light nuclei. For this imitation we need to estimate a suitable late freeze-out. This we do by fitting the afterburner effect for protons by means of the late freeze-out. We choose protons because they are closely related to the light nuclei. The basic idea behind such imitation is as follows. If the afterburner effect for protons can be imitated by the late freeze-out, we anticipate that the same late freeze-out can do the same for light nuclei.

In the 3FD calculations a differential, i.e., cell-by-cell, freeze-out is implemented [53]. The freeze-out procedure starts when the local energy density drops down to the freeze-out value $\varepsilon_{\rm frz}$, which is conventionally taken to be 0.4 GeV/fm^3 for all collision energies and centralities.

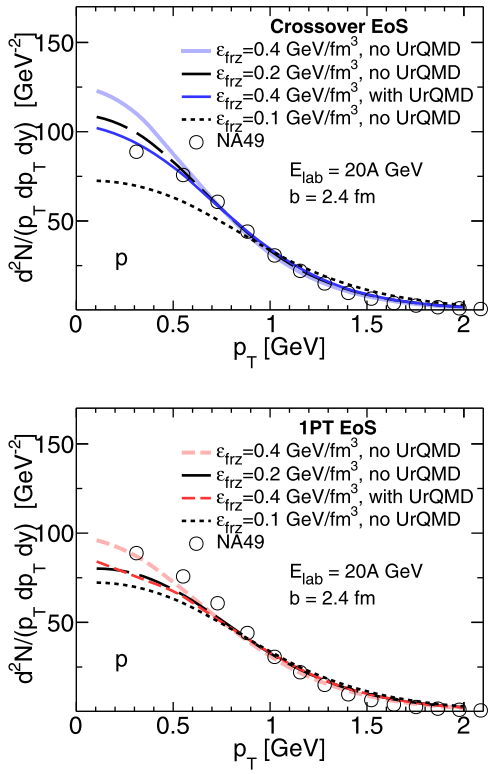

FIG. 1. Transverse-momentum spectra of protons in central Au + Au collisions at collision energy of $E_{\rm lab} = 20A$ GeV calculated with the crossover (upper panel) and 1PT EoS's (lower panel). Results of the THESEUS simulations (without the subsequent UrQMD afterburner) based on the 3FD calculations with different freeze-out energy densities $\varepsilon_{\rm frz} = 0.1$, 0.2, and 0.4 GeV/fm^3 are shown. The conventional results for 3FD with $\varepsilon_{\rm frz} = 0.4$ GeV/fm^3 and the subsequent UrQMD afterburner are also presented. Experimental data are from the NA49 Collaboration [55].

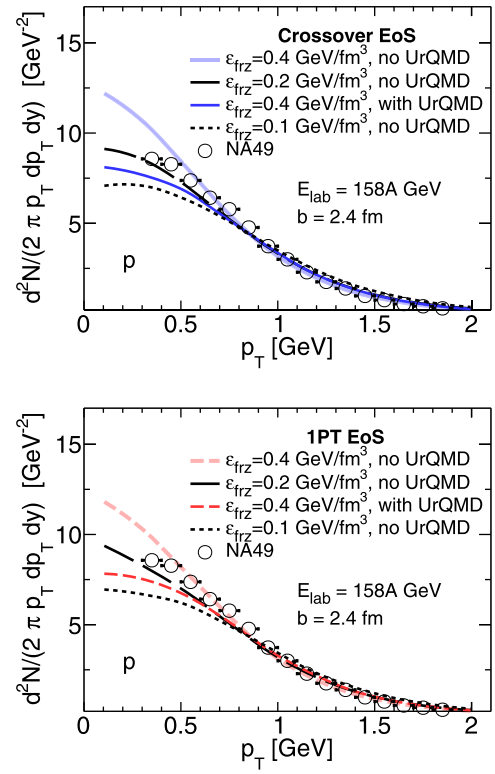

FIG. 2. The same as in Fig. 1 but for $E_{\rm lab} = 158A$ GeV. Experimental data are from the NA49 Collaboration [56].

The freeze-out criterion is checked in the analyzed cell and in eight surrounding cells. If the criterion is met in all cells and if the analyzed cell is adjacent to the vacuum (i.e., if at least one of the surrounding cells is "empty"[1]), then the considered cell is counted as frozen out. The latter condition prevents formation of bubbles of frozen-out matter inside the still hydrodynamically evolving matter. Thus, the actual energy density of a frozen-out cell turns out to be lower than $\varepsilon_{\rm frz}$. Therefore, $\varepsilon_{\rm frz}$ has a meaning of a "trigger" value that indicates possibility of the freeze-out. This freeze-out pattern is similar to the process of expansion of a compressed and heated fluid into vacuum, mechanisms of which were studied both experimentally and theoretically; see discussion in Ref. [53]. The freeze-out is associated with evaporation from the surface of the expanding fluid.

In Figs. 1 and 2, transverse-momentum spectra of protons in central Au + Au collisions at collision energies of $E_{\rm lab} = 20A$ and $158A$ GeV are shown. These spectra are calculated by means of THESEUS simulations without the subsequent UrQMD afterburner, similarly to the light-nuclei simulations, based on the 3FD calculations with different freeze-out energy densities $\varepsilon_{\rm frz} = 0.1$, 0.2, and 0.4 GeV/fm^3. The conventional results for 3FD with $\varepsilon_{\rm frz} = 0.4$ GeV/fm^3 and the subsequent UrQMD afterburner are also presented. The results are presented in linear scale in order to better resolve the low p_T region, which is mostly affected by the afterburner effect [54].

As seen from Figs. 1 and 2, the late freeze-out with the energy density $\varepsilon_{\rm frz} = 0.2$ GeV/fm^3 approximately reproduces the afterburner effect in midrapidity proton p_T spectra at both collision energies and in different EoS scenarios. The reproduction of the high-p_T spectra is also good, though it is hardly seen in the linear scale. We avoid fine tuning of the late freeze-out because this is only an imitation of the afterburner.

The effect of the late freeze-out on rapidity distribution of net-protons is demonstrated in Fig. 3. The late freeze-out with $\varepsilon_{\rm frz} = 0.2$ GeV/fm^3 reasonably well reproduces results for conventional freeze-out with the subsequent UrQMD afterburner in the midrapidity region. The reproduction for $E_{\rm lab} = 20A$ GeV (not shown) is even better, as can be expected from Fig. 1. However, the freeze-out energy density $\varepsilon_{\rm frz} = 0.2$ GeV/fm^3 is not that good in imitating the afterburner effect at forward/backward rapidities; see Fig. 3. Below we use this late freeze-out with $\varepsilon_{\rm frz} = 0.2$ GeV/fm^3 for calculations of light nuclei for all considered collision energies and centralities.

As seen from Fig. 3, the rapidity-integrated net-proton yield $\varepsilon_{\rm frz} = 0.1$ GeV/fm^3 is visibly larger than that at higher $\varepsilon_{\rm frz}$ because the rapidity distribution at 0.1 GeV/fm^3 extends

[1]Frozen-out cells are removed from the hydrodynamical evolution.

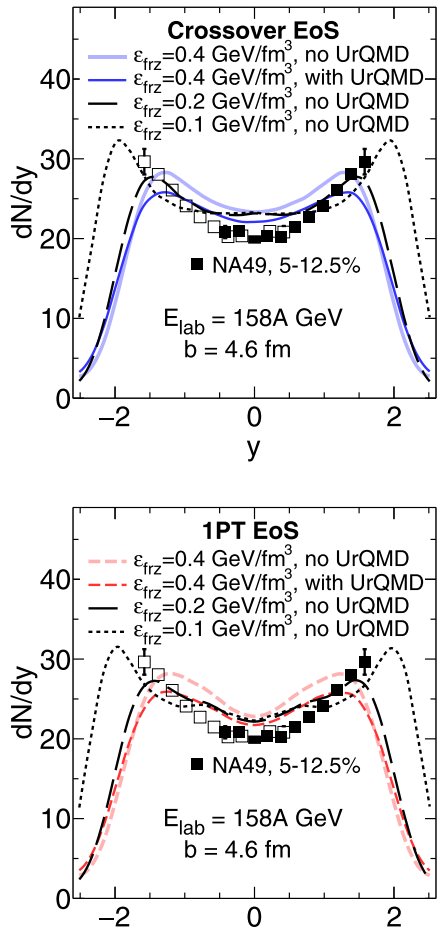

FIG. 3. Rapidity distributions of net protons in central ($b = 2.4$ fm) Pb + Pb collisions at $E_{\rm lab} = 158A$ GeV calculated with the crossover EoS (upper panel) and the 1PT EoS (lower panel). Results of the THESEUS simulations (without the subsequent UrQMD afterburner) based on the 3FD calculations with different freeze-out energy densities $\varepsilon_{\rm frz} = 0.1$, 0.2, and 0.4 GeV/fm^3 are shown. The conventional results for 3FD with $\varepsilon_{\rm frz} = 0.4$ GeV/fm^3 and the subsequent UrQMD afterburner are also presented. Experimental data are from the NA49 Collaboration [57].

to larger forward/backward rapidities. The reason is that only participant test particles (at the Lagrangian step of 3FD) are recoded in the 3FD output and thus transferred to THESEUS. The spectator test particles,[2] containing bound nuclear matter, are omitted. At the late freeze-out, the participant region expands, involving more and more former spectators. Therefore, the total number of net-proton participants increases.

A. Rapidity distributions

We start with analysis of rapidity distributions of light nuclei; see Figs. 4 and 5. We compare our results with NA49 data [43], as well as with the 3FD coalescence results [51].

[2]Those whose proper energy per baryon charge of is less than the nucleon mass.

Recall that the light nuclei are simulated without the afterburner stage. To illustrate once again the expected effect of the afterburner stage, we present results of the simulations with conventional freeze-out, $\varepsilon_{\rm frz} = 0.4$ GeV/fm^3, and late freeze-out, $\varepsilon_{\rm frz} = 0.2$ GeV/fm^3, which imitate the afterburner stage. As can be seen, in the midrapidity region the THESEUS results systematically overestimate the data on light-nuclei yields. The late freeze-out somewhat improves agreement with the data but not completely. The extent of this agreement depends on the EoS. The crossover EoS results in better agreement with data than the 1PT EoS. It is surprising that reproduction of the ^{3}He data turns out to be better than that of the data on deuterons, in spite of ^{3}He being a heavier nucleus.

The energy of $E_{\rm lab} = 80A$ GeV drops out of the systematics. The disagreement with data at $80A$ GeV is larger than at neighboring energies of $40A$ and $158A$ GeV, as if the clustering is additionally suppressed at $80A$ GeV. The 3FD coalescence [51], also presented in Figs. 4 and 5 by short-dashed lines, much better reproduces the data because the coalescence coefficients were tuned for each collision energy and each light nucleus. Nevertheless, the THESEUS simulations result in good agreement with the dependence of light-nuclei production on the collision energy and light-nucleus mass. This agreement does not need any additional tuning parameters, i.e., in addition to those used for description of all other hadron yields, in contrast to the 3FD coalescence.

Results of simulations without the contribution of low-lying resonances of ^{4}He are also displayed Figs. 4 and 5 by long-dashed lines. The effect of low-lying resonances of the ^{4}He system in the midrapidity region is small at the considered collision energies, as already mentioned in Ref. [38]. However, it is essential in the fragmentation regions. These feed-down contributions from decays of unstable ^{4}He are compatible with the results obtained within the statistical model [34].

For comparison, the rapidity distributions of net protons are presented in Fig. 6. The net protons are reproduced much better. The UrQMD afterburner slightly reduces net-proton yield in the midrapidity region and drives it to even better agreement with data. This reduction rises with the collision energy increase. Still it is much smaller than that for light nuclei, i.e., the difference between calculations with $\varepsilon_{\rm frz} = 0.2$ and 0.4 GeV/fm^3. The crossover EoS again results in better agreement with available data than the 1PT EoS. Apparently, small inconsistency with proton data transforms in large inconsistency with data on light nuclei.

The rapidity distributions of net protons and light nuclei are quite different. While the net-proton distributions at $E_{\rm lab} = 20A$–$80A$ GeV reveal a peak or a shallow dip at midrapidities, the distributions of light nuclei demonstrate high maxima at forward/backward rapidities. These maxima are formed because the matter at the periphery of colliding system (i.e., at forward/backward rapidities) is colder than in its center (i.e., in midrapidity) and hence the relative abundances of light nuclei become large. Only small humps in the midrapidity of light-nuclei distributions remind about midrapidity peaks in the net protons.

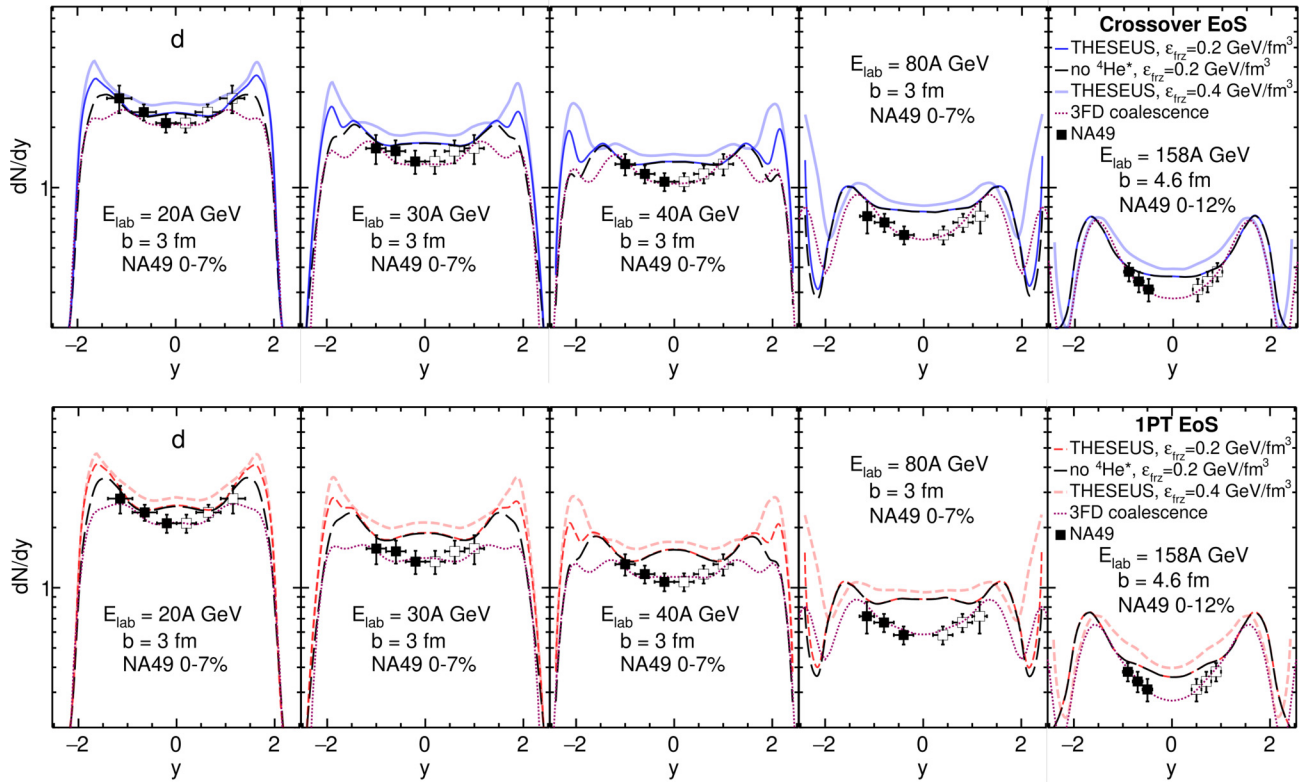

FIG. 4. Rapidity distributions of deuterons in central Pb + Pb collisions at collision energies of $E_{\rm lab} = 20A$–$158A$ GeV calculated with the crossover EoS (upper raw of panels) and the 1PT EoS (lower raw of panels). Results of THESEUS simulations with the conventional freeze-out, $\varepsilon_{\rm frz} = 0.4$ GeV/fm^3, and the late freeze-out, $\varepsilon_{\rm frz} = 0.2$ GeV/fm^3, are displayed. Results of the simulations without contribution of low-lying resonances of ^{4}He and the 3FD coalescence results [51] are also presented. Experimental data are from the NA49 Collaboration [43].

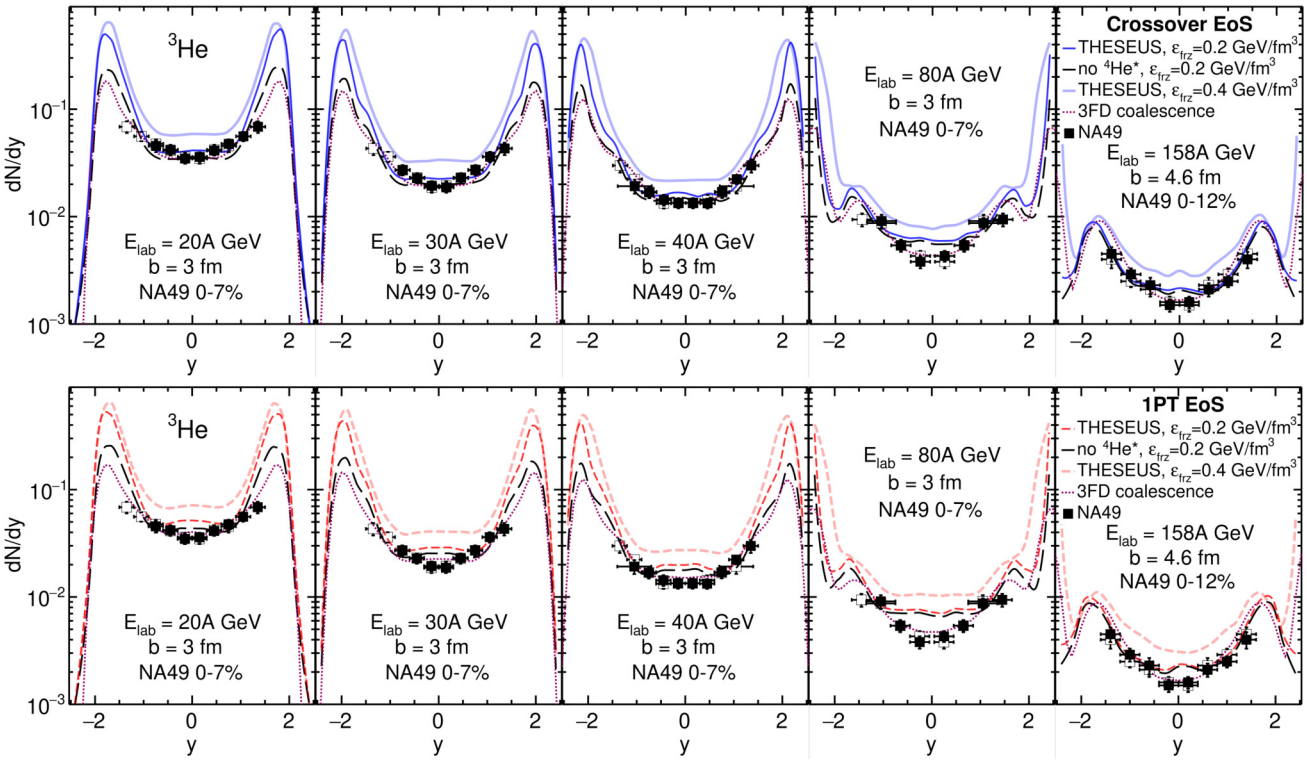

FIG. 5. The same as in Fig. 4 but for the ^{3}He nuclei.

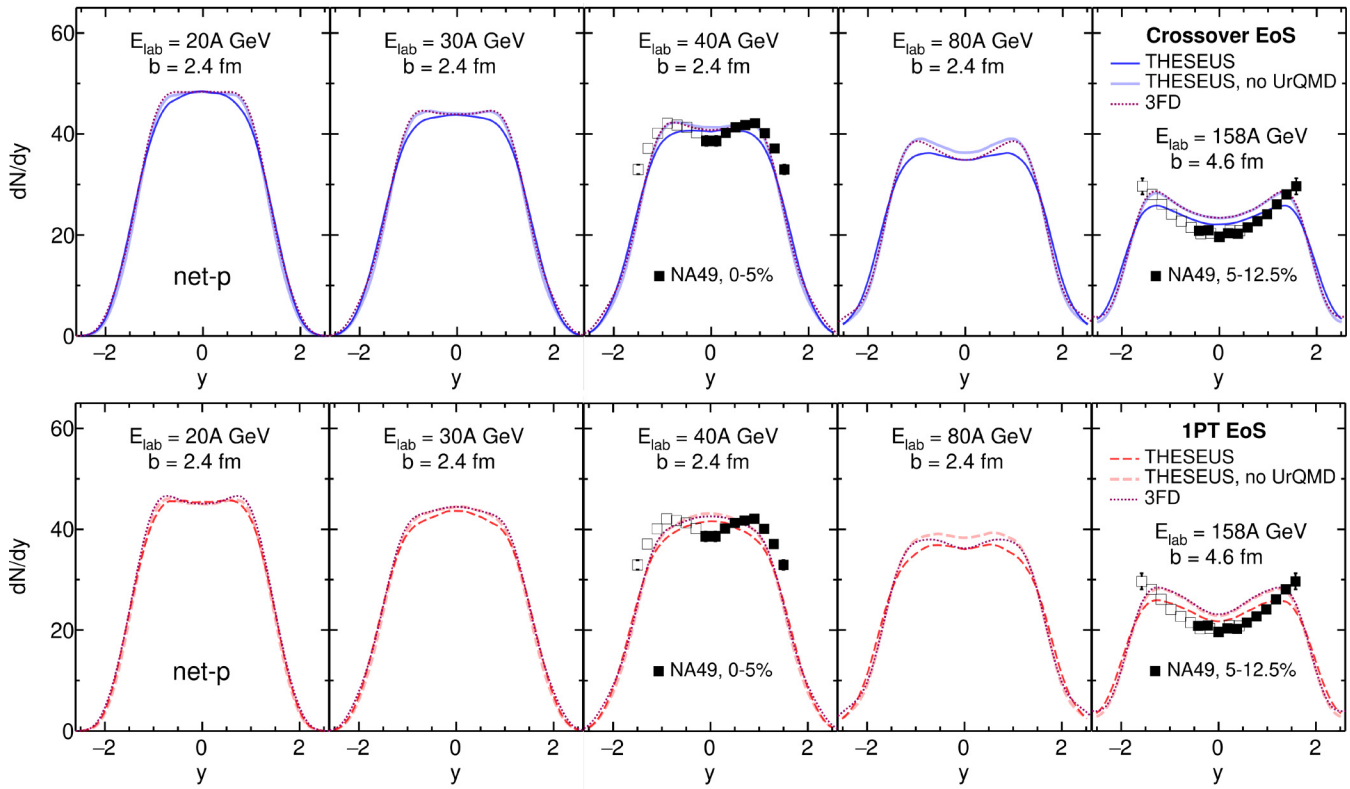

FIG. 6. The same as in Fig. 4 but for net protons in central Pb + Pb collisions. Results of simulations without the UrQMD afterburner and the 3FD results [51] are also displayed. Experimental data are from the NA49 Collaboration [57].

B. Transverse-momentum spectra

Transverse-mass spectra of deuterons and tritons at midrapidity in central Pb + Pb collisions at collision energies of $E_{\rm lab} = 20A$–$158A$ GeV, measured by the NA49 Collaboration [43], are compared with the results of the THESEUS simulations in Fig. 7. Only the calculations with the crossover EoS are shown because the 1PT scenario results in a similar picture, where agreement with data is even slightly worse. Again, results of THESEUS simulations with conventional freeze-out, $\varepsilon_{\rm frz} = 0.4$ GeV/fm^3, and late freeze-out, $\varepsilon_{\rm frz} = 0.2$ GeV/fm^3, are displayed. The 3FD coalescence results [51] are also shown.

The slopes of the 3FD coalescence and THESEUS (with conventional freeze-out) spectra are very similar, in spite of being obtained within different approaches. This is because the coalescence and thermodynamical expressions for the light-nuclei yields are very similar except for the tunable coalescence coefficients implied in the coalescence approach, which control the overall normalization. The agreement of these spectra with the NA49 data is far from being perfect. The normalization of the light-nuclei spectra is strongly overestimated within the THESEUS with conventional freeze-out. Imitation of the afterburner (THESEUS with $\varepsilon_{\rm frz} = 0.2$ GeV/fm^3) somewhat improves the normalization at low $m_T - m$ but worsens agreement with the slopes. The overall normalization of the 3FD-coalescence spectra is better but this is achieved by tuning the coalescence parameters.

The late freeze-out makes slopes of the m_T spectra less steep, which is an expected effect of the afterburner [54]. This effect of the afterburner on proton spectra is demonstrated in Fig. 8. For the protons, it is the UrQMD afterburner after the conventional 0.4 GeV/fm^3 freeze-out that reduces the slope, rather than the late freeze-out for light nuclei. In the case of the late freeze-out, this flattening of the slope is a result of an increase of the radial-flow velocity over time.

The proton transverse-mass spectra at midrapidity in central Pb + Pb collisions at the same collision energies are presented in Fig. 8. Again, results of 3FD simulations are also displayed. As seen, the afterburner (THESEUS curves in Fig. 8) improves agreement with the NA49 data [55] at low $m_T - m$ as compared with 3FD, but the slopes disagree with the data. However, this disagreement is much smaller than that for light nuclei in Fig. 7.

The calculated ^{3}He spectra are closer to the data than the deuteron data, which is again surprising. The spectra slopes are better reproduced at lower energies. Together with better agreement with rapidity distributions of light nuclei at lower energies, this may suggest that THESEUS is more suitable for simulating light nuclei at NICA and FAIR energies.

Again we may conclude that small disagreement with proton data transforms into a large disagreement with data on light nuclei. In particular, slightly better reproduction of the proton data within the crossover scenario, as compared with the 1PT one (see Figs. 6 and 8), results in noticeably better agreement with data on light nuclei; cf. Fig. 5.

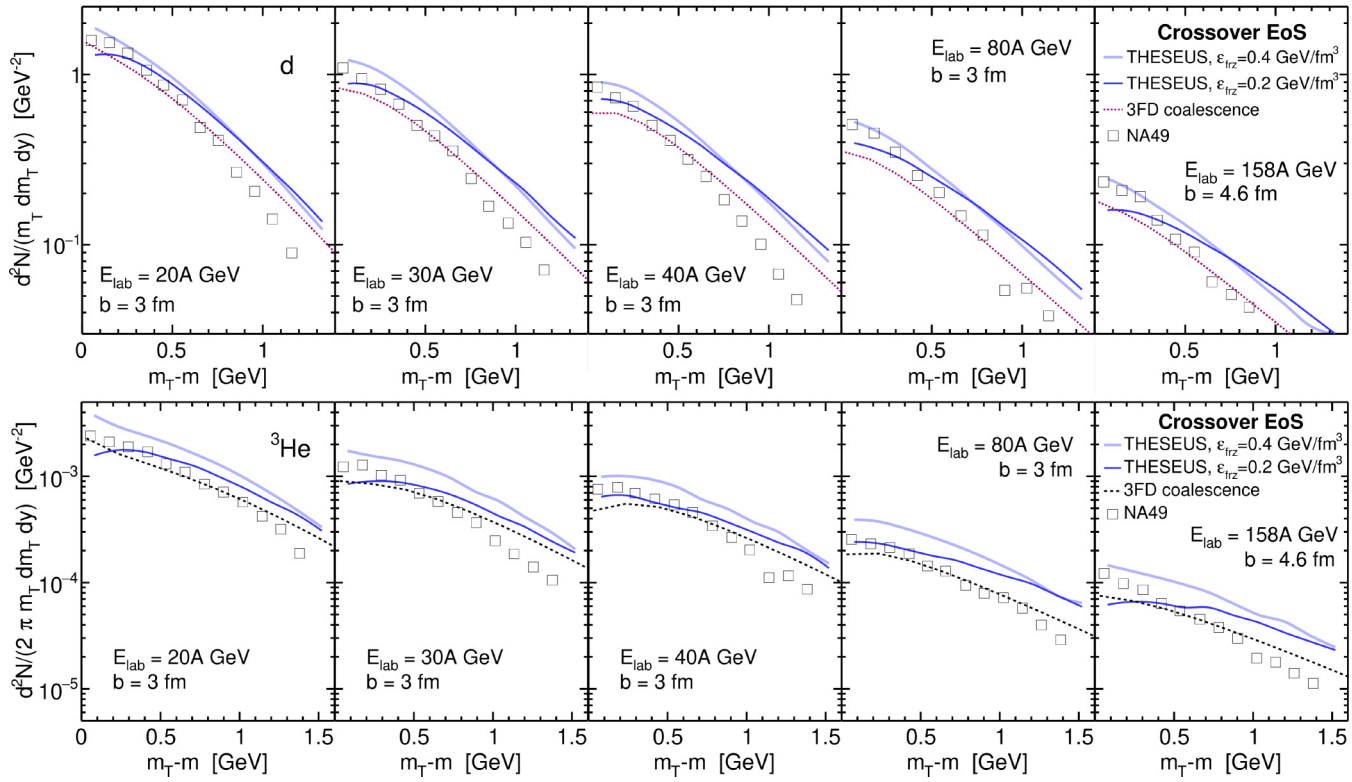

FIG. 7. Transverse-mass spectra of deuterons (upper raw of panels) and tritons (lower raw of panels) in central Pb + Pb collisions at collision energies of $E_{lab} = 20A$–$158A$ GeV calculated with the crossover EoS. Results of THESEUS simulations with conventional freeze-out, $\varepsilon_{frz} = 0.4$ GeV/fm^3, and late freeze-out, $\varepsilon_{frz} = 0.2$ GeV/fm^3, are displayed. The 3FD coalescence results [51] are also shown. NA49 data are from Ref. [43].

The 3FD predictions overestimate the high-m_T ends of the spectra because of finiteness of the considered system. Even abundant hadronic probes become rare at high momenta. Therefore, their treatment on the basis of the grand canonical ensemble results in overestimation of their yields. Moreover, the more rare a probe is, the more strongly its high-p_T end of the spectrum is suppressed due to restrictions of the canonical ensemble. Therefore, the light-nuclei high-p_T spectra are more strongly overestimated than the proton spectra. The UrQMD afterburner, as implemented in THESEUS [38,44], does not improve the high-p_T description. The reason is that the grand canonical distributions are sampled in the particlization procedure, rather than the canonical or microcanonical ones. Thus, the high-p_T overestimation persists. Of course, it is difficult to indicate how much of this overestimation is due to the grand canonical treatment, and not to the shortcomings of the model.

We did not tune the 3FD model to reproduce the data on light nuclei, in particular, the m_T spectra. The poor agreement with the data on the m_T spectra is the price paid for the intention to reproduce numerous data in a wide range of collision energies with the same set of parameters described in Ref. [40].

C. Yield ratios of light nuclei

Energy dependence of d/p, t/p, and t/d midrapidity ratios for central collisions are presented in Fig. 9. Protons in these ratios do not contain feed-down from weak decays, in accordance with the experimental procedure [31,32]. As can be seen, the model reproduces the energy dependence of experimental data [32] but systematically overestimates the values of these ratios. This reproduction is similar to that within the statistical model [32].

The yield ratio of light nuclei, $N_t N_p/N_d^2$, has been suggested as a probe of the neutron density fluctuations associated with the first-order phase transition [58,59]. Later it was also associated with the possible critical point of the hot and baryon-rich QCD matter [3–5]. Near the critical point, this ratio increases monotonically with the nucleon density correlation length [5]; besides, production of ^{3}He may increase because of enhanced preclustering and subsequent decay of ^{4}He-like clusters [3,4]. In turn, this may result in a maximum in the $N_t N_p/N_d^2$ ratio near the critical point. Recent data on this ratio [32] show a nonmonotonic behavior with a peak located around 20–30 GeV (see Fig. 10), which might indicate passing through either the first-order phase transition or critical point at this collision energy.

Energy dependence of the midrapidity $N(t) \times N(p)/N^2(d)$ ratio in central Au + Au and Pb + Pb collisions is presented in Fig. 10. Simulations were performed at $b = 4$ fm for Au + Au, and at $b = 3$ fm ($\sqrt{s_{NN}} < 17.4$ GeV) and $b = 4.6$ fm ($\sqrt{s_{NN}} = 17.4$ GeV) for Pb + Pb in rapidity bin $|y| < 0.5$ with the crossover and 1PT EoS's. The proton yields does not include contribution from the weak-decay feed-down.

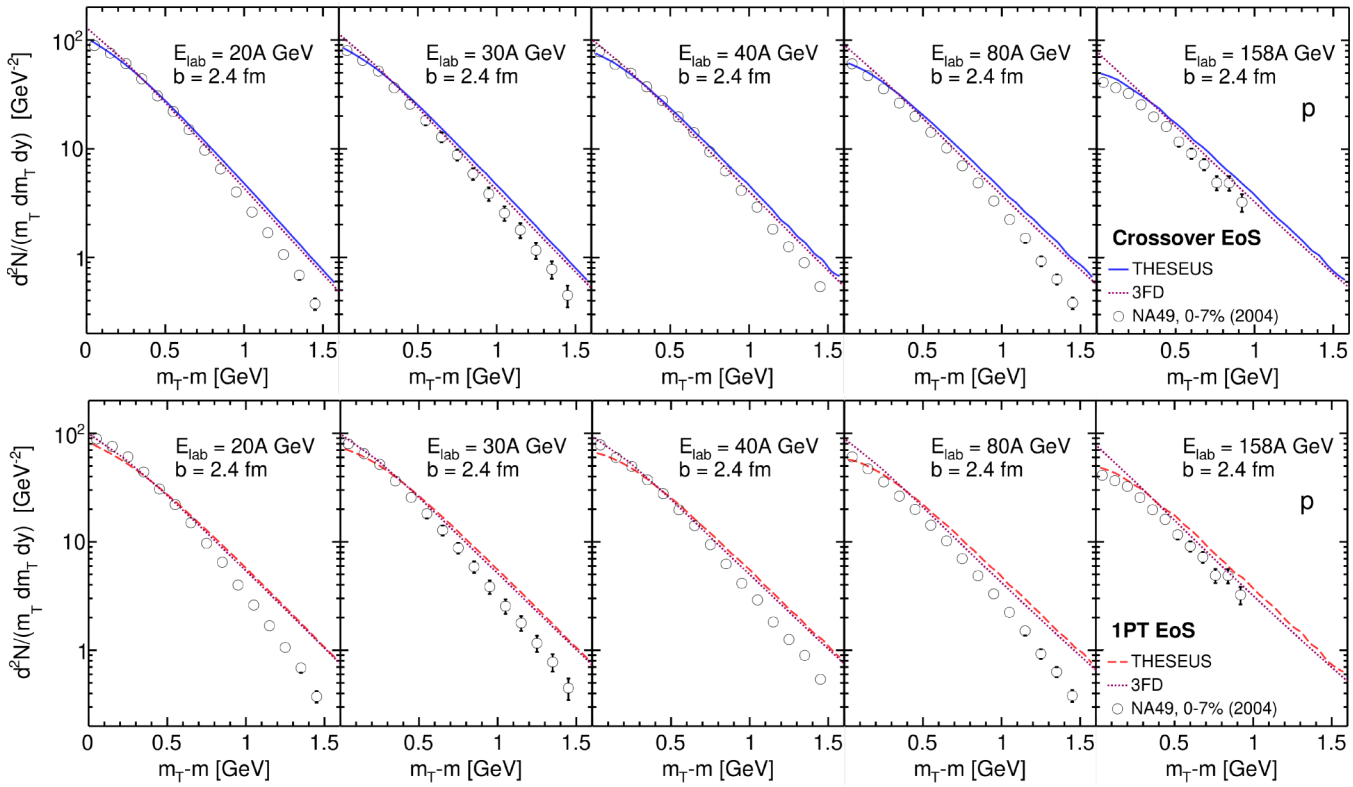

FIG. 8. The same as in Fig. 7 but for protons calculated with the crossover EoS (upper row of panels) and the 1PT EoS (lower row of panels). Results of conventional THESEUS simulations (i.e., with the UrQMD afterburner) and the 3FD results [51] are displayed. NA49 data are from Ref. [55].

This weak-decay feed-down was determined by the UrQMD simulation at the afterburner stage, i.e., in the same way as the proton feed-down correction was done in the preliminary STAR data [35]. In the final STAR data [32] (filled circles in Fig. 10), the feed-down correction was done by experimental means. The STAR Collaboration concludes that the UrQMD

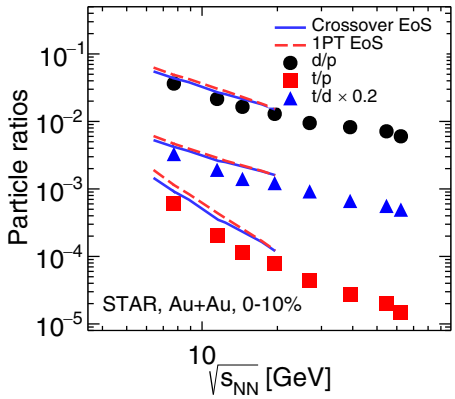

FIG. 9. Energy dependence of d/p, t/p, and t/d midrapidity ratios for central (0–10%) Au + Au collisions. Simulations were performed at $b = 4$ fm for Au + Au and at $b = 3$ fm for Pb + Pb in rapidity bin $|y| < 0.5$. Results with the crossover and 1PT EoS's are presented. Results of the calculations are compared with STAR data [32] for central (0–10%) Au + Au collisions.

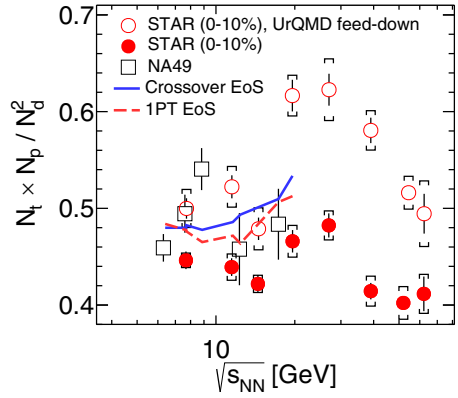

FIG. 10. Energy dependence of the midrapidity light-nuclei-yield ratio $N(t) \times N(p)/N^2(d)$ in central Au + Au and Pb + Pb collisions. Simulations were performed at $b = 4$ fm for Au + Au, and at $b = 3$ fm ($\sqrt{s_{NN}} < 17.4$ GeV) and $b = 4.6$ fm ($\sqrt{s_{NN}} = 17.4$ GeV) for Pb + Pb in rapidity bin $|y| < 0.5$. $N(p)$ is related to protons without feed-down from weak decays. Results of the calculations are compared with STAR preliminary data [35] (open circles), where weak-decay feed-down into proton yield was determined by means of the UrQMD simulations, and with final data [32] (filled circles), with the weak-decay feed-down determined by experimental means, for central (0–10%) Au + Au collisions. The experimental results extracted from the NA49 data on Pb + Pb collisions (0–7% at 20*A*–80*A* GeV and 0–12% at 158*A* GeV) [43] are also displayed (open boxes).

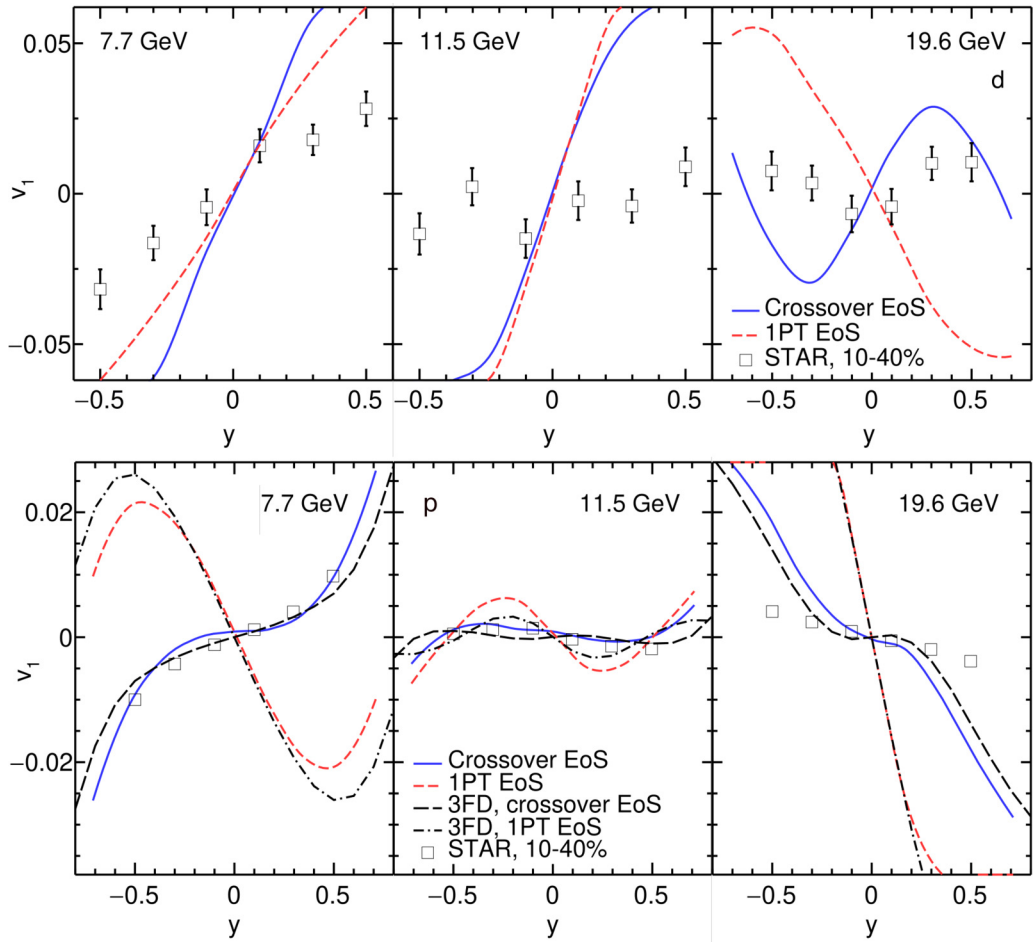

FIG. 11. Directed flow of deuterons (upper row of panels) and protons (lower row of panels) as functions of rapidity in semicentral ($b = 6$ fm) Au + Au collisions at collision energies of $\sqrt{s_{NN}} = 7.7$, 11.5, and 19.6 GeV calculated with the crossover and 1PT EoS's. Results of the 3FD simulations [61], i.e., without the UrQMD afterburner, are also presented for protons. Experimental STAR data for deuterons are from Ref. [62] and those for protons are from Ref. [63].

simulation underestimates the proton feed-down contributions from weak decays. If so, our simulations suffer from the same shortcoming of UrQMD. Therefore, we also present these preliminary data [35] in Fig. 10 for comparison.

The calculated $N(t) \times N(p)/N^2(d)$ ratios overestimate the final STAR data both for the crossover and 1PT EoS's. At the same time they are, as a rule, below preliminary STAR data. Therefore, the overestimation can be related to the aforementioned shortcoming of UrQMD. The calculated ratios show an increase as the energy approaches 20 GeV, in spite of absence of the critical point in the considered EoS's. This is not an effect of a special tune of the model parameters. As described above, there was no such special tune. This increase can be also an artifact of the underestimation of the proton feed-down contributions from weak decays at the UrQMD stage. Indeed, from Fig. 10 we can see that the difference between the preliminary and final STAR data becomes larger at $\sqrt{s_{NN}} \geqslant 20$ GeV as compared with that at lower energies.

We may conclude that the feed-down contributions of hyperon weak decays should be carefully subtracted from the proton yield in order for the calculated $N(t) \times N(p)/N^2(d)$ ratio to serve as probe of production characteristics of light nuclei and the structure of the QCD phase diagram. The UrQMD is not quite accurate for such subtraction. A similar conclusion was made in Ref. [60].

D. Directed flow

The directed flow (v_1) is one of the most delicate characteristics of the heavy-ion collisions. Nevertheless, we calculated the deuteron v_1 relying on relatively successful description of the proton v_1 within the 3FD model [61]. This is a straightforward calculation because light nuclei are treated on an equal basis with other hardrons in the present approach.

The directed flow of deuterons (upper raw of panels in Fig. 11), calculated for late freeze-out (i.e., $\varepsilon_{\rm frz} = 0.2$ GeV/fm^3) to imitate the afterburner effect, is shown and compared with STAR data [62] in Fig. 11. The directed flow of protons (lower row of panels in Fig. 11) is also presented for comparison. In these simulations, experimental acceptance [62] was used: $0.4 < p_T < 2.0$ GeV/c for protons and $0.8 < p_T < 4.0$ GeV/c for deuterons. To illustrate the effect of

the afterburner, results of the 3FD simulations of protons v_1 are displayed. As seen, the afterburner insignificantly changes proton v_1. The "afterburner" effect in deuteron v_1 (not displayed) is sightly stronger but still not dramatic.

The directed flow of deuterons is quite different from the proton one. As can be seen, the deuteron v_1 is stronger than the proton v_1. Even signs of the midrapidity slopes of the deuteron and proton $v_1(y)$ are not always the same. The crossover and 1PT EoS's predict different v_1, which is not surprising because the proton $v_1(y)$ are also very different for these EoS's. While the crossover EoS well reproduces the data on the proton v_1, overall reproduction of the deuteron data is much worse than that for protons. Nevertheless, the order of magnitude of the deuteron v_1 is comparable with the data, except at the energy of 11.5 GeV, where the deuteron v_1 collapses similarly to the proton v_1.

Contrary to our naive expectation, the reproduction of the proton directed flow does not guarantee a good description of that for light nuclei. The nucleon directed flow, represented by the proton one, measures azimuthal asymmetry of the baryon current because all baryonic resonances decay into nucleons after the freeze-out. The light-nuclei directed flow does not contain the contribution of the baryonic resonances in accordance to the thermodynamic approach. It additionally depends on the azimuthal asymmetry of the temperature and baryon density because denser and colder regions give larger contributions to the light-nuclei production. All these make the light-nuclei directed flow and even its midrapidity slope different from those of the proton. In Sec. III A, we already discussed how inhomogeneity of the temperature distribution along the beam direction makes rapidity distributions of net protons and light nuclei quite different.

The afterburner stage may essentially change the light-nuclei flow because of decays and reproduction of light nuclei, as realized in, e.g., the SMASH [23,24] and PHQMD [26,27] transport models. These processes may result in deviation from the kinetic equilibrium. Our imitation of the afterburner by means of the late freeze-out does not violate the kinetic equilibrium.

IV. SUMMARY

Simulations of the light-nuclei production in relativistic heavy-ion collisions within the updated THESEUS [38] event generator were performed for Pb + Pb and Au + Au collisions in the collision energy range of $\sqrt{s_{NN}} = 6.4$–19.6 GeV. The results were compared with available data from the NA49 and STAR Collaborations. The updated THESEUS treats the light-nuclei production within the thermodynamical approach on an equal basis with hadrons. The only additional parameter related to the light nuclei is the energy density of the late freeze-out, $\varepsilon_{\text{late frz}} = 0.2$ GeV/fm^3, which is the same for all collision energies, centralities, and combinations of colliding nuclei. For comparison, the conventional freeze-out energy density in 3FD is $\varepsilon_{\text{frz}} = 0.4$ GeV/fm^3, that is also universal. This late freeze-out imitates the afterburner stage of the collision because the light nuclei are not subjected to the UrQMD afterburner. $\varepsilon_{\text{late frz}}$ is not a free parameter; it is chosen using the condition of the best reproduction of the proton p_T spectrum after the UrQMD afterburner by the spectrum at the late freeze-out without the afterburner.

The updated generator revealed imperfect but reasonable reproduction of the data on bulk observables of the light nuclei, especially the functional dependence on the collision energy and light-nucleus mass. It is important that this reproduction is achieved with a single universal additional parameter related to late freeze-out. The collective directed flow of light nuclei turns out to be more involved. Apparently, it requires an explicit treatment of the afterburner evolution of light nuclei with due account of violation of the kinetic equilibrium.

Various ratios, d/p, t/p, t/d, and $N(t) \times N(p)/N^2(d)$, were also considered. We conclude that the feed-down contributions of weak decays should be carefully subtracted from the proton yield in order for the calculated $N(t) \times N(p)/N^2(d)$ ratio to serve as probe of production characteristics of light nuclei and the structure of the QCD phase diagram. The UrQMD is not quite accurate for such subtraction.

Imperfect reproduction of the light-nuclei data leaves room for medium effects in production of light nuclei, which were advanced in Refs. [64,65]; see also [66].

ACKNOWLEDGMENTS

We are grateful to David Blaschke for convincing us to apply the thermodynamic approach to modeling the light-nuclei production in heavy-ion collisions. We are especially grateful to Iurii Karpenko, without whose help and expertise this work would hardly have been possible. Useful discussions with V. Kireyeu are gratefully acknowledged. This work was carried out using computing resources of the supercomputer "Govorun" at JINR.

[1] J. Adam *et al.* (STAR Collaboration), Nonmonotonic Energy Dependence of Net-Proton Number Fluctuations, Phys. Rev. Lett. **126**, 092301 (2021).

[2] M. A. Stephanov, Non-Gaussian Fluctuations near the QCD Critical Point, Phys. Rev. Lett. **102**, 032301 (2009).

[3] E. Shuryak and J. M. Torres-Rincon, Baryon preclustering at the freeze-out of heavy-ion collisions and light-nuclei production, Phys. Rev. C **101**, 034914 (2020).

[4] E. Shuryak and J. M. Torres-Rincon, Light-nuclei production and search for the QCD critical point, Eur. Phys. J. A **56**, 241 (2020).

[5] K. J. Sun, F. Li and C. M. Ko, Effects of QCD critical point on light nuclei production, Phys. Lett. B **816**, 136258 (2021).

[6] J. Steinheimer and J. Randrup, Spinodal Amplification of Density Fluctuations in Fluid-Dynamical Simulations of Relativistic Nuclear Collisions, Phys. Rev. Lett. **109**, 212301 (2012).

[7] J. Steinheimer, L. Pang, K. Zhou, V. Koch, J. Randrup, and H. Stoecker, A machine learning study to identify spinodal clumping in high energy nuclear collisions, J. High Energy Phys. 12 (2019) 122.

[8] V. V. Skokov and D. N. Voskresensky, Hydrodynamical description of a hadron-quark first-order phase transition, JETP Lett. **90**, 223 (2009).

[9] V. V. Skokov and D. N. Voskresensky, Hydrodynamical description of first-order phase transitions: Analytical treatment and numerical modeling, Nucl. Phys. A **828**, 401 (2009).

[10] J. Randrup, Phase transition dynamics for baryon-dense matter, Phys. Rev. C **79**, 054911 (2009).

[11] V. N. Russkikh, Y. B. Ivanov, Y. E. Pokrovsky, and P. A. Henning, Analysis of intermediate-energy heavy ion collisions within relativistic mean field two fluid model, Nucl. Phys. A **572**, 749 (1994).

[12] Y. B. Ivanov, V. N. Russkikh, and V. D. Toneev, Relativistic heavy-ion collisions within three-fluid hydrodynamics: Hadronic scenario, Phys. Rev. C **73**, 044904 (2006).

[13] H. Liu, D. Zhang, S. He, K. j. Sun, N. Yu, and X. Luo, Light nuclei production in Au+Au collisions at $\sqrt{s_{\rm NN}} = 5$–200 GeV from JAM model, Phys. Lett. B **805**, 135452 (2020).

[14] L. Zhu, C. M. Ko, and X. Yin, Light (anti-)nuclei production and flow in relativistic heavy-ion collisions, Phys. Rev. C **92**, 064911 (2015).

[15] J. Steinheimer, K. Gudima, A. Botvina, I. Mishustin, M. Bleicher, and H. Stocker, Hypernuclei, dibaryon and antinuclei production in high energy heavy ion collisions: Thermal production versus coalescence, Phys. Lett. B **714**, 85 (2012).

[16] Z. J. Dong, G. Chen, Q. Y. Wang, Z. L. She, Y. L. Yan, F. X. Liu, D. M. Zhou and B. H. Sa, Energy dependence of light (anti)nuclei and (anti)hypertriton production in the Au-Au collision from $\sqrt{s_{NN}} = 11.5$ to 5020 GeV, Eur. Phys. J. A **54**, 144 (2018).

[17] S. Sombun, K. Tomuang, A. Limphirat, P. Hillmann, C. Herold, J. Steinheimer, Y. Yan, and M. Bleicher, Deuteron production from phase-space coalescence in the UrQMD approach, Phys. Rev. C **99**, 014901 (2019).

[18] P. Hillmann, K. Käfer, J. Steinheimer, V. Vovchenko, and M. Bleicher, Coalescence, the thermal model and multifragmentation: the energy and volume dependence of light nuclei production in heavy ion collisions, J. Phys. G: Nucl. Part. Phys. **49**, 055107 (2022).

[19] W. Zhao, C. Shen, C. M. Ko, Q. Liu, and H. Song, Beam-energy dependence of the production of light nuclei in Au+Au collisions, Phys. Rev. C **102**, 044912 (2020).

[20] W. Zhao, K. j. Sun, C. M. Ko, and X. Luo, Multiplicity scaling of light nuclei production in relativistic heavy-ion collisions, Phys. Lett. B **820**, 136571 (2021).

[21] D. Oliinychenko, Overview of light nuclei production in relativistic heavy-ion collisions, Nucl. Phys. A **1005**, 121754 (2021).

[22] J. Weil, V. Steinberg, J. Staudenmaier, L. G. Pang, D. Oliinychenko, J. Mohs, M. Kretz, T. Kehrenberg, A. Goldschmidt, B. Bäuchle *et al.*, Particle production and equilibrium properties within a new hadron transport approach for heavy-ion collisions, Phys. Rev. C **94**, 054905 (2016).

[23] D. Oliinychenko, L. G. Pang, H. Elfner, and V. Koch, Microscopic study of deuteron production in PbPb collisions at $\sqrt{s} = 2.76$ TeV via hydrodynamics and a hadronic afterburner, Phys. Rev. C **99**, 044907 (2019).

[24] J. Staudenmaier, D. Oliinychenko, J. M. Torres-Rincon, and H. Elfner, Deuteron production in relativistic heavy ion collisions via stochastic multiparticle reactions, Phys. Rev. C **104**, 034908 (2021).

[25] J. Aichelin, E. Bratkovskaya, A. Le Fèvre, V. Kireyeu, V. Kolesnikov, Y. Leifels, V. Voronyuk, and G. Coci, Parton-hadron-quantum-molecular dynamics: A novel microscopic n-body transport approach for heavy-ion collisions, dynamical cluster formation, and hypernuclei production, Phys. Rev. C **101**, 044905 (2020).

[26] S. Gläßel, V. Kireyeu, V. Voronyuk, J. Aichelin, C. Blume, E. Bratkovskaya, G. Coci, V. Kolesnikov, and M. Winn, Cluster and hypercluster production in relativistic heavy-ion collisions within the parton-hadron-quantum-molecular-dynamics approach, Phys. Rev. C **105**, 014908 (2022).

[27] E. Bratkovskaya, S. Glässel, V. Kireyeu, J. Aichelin, M. Bleicher, C. Blume, G. Coci, V. Kolesnikov, J. Steinheimer, and V. Voronyuk, Midrapidity cluster formation in heavy-ion collisions, arXiv:2208.11802.

[28] K. J. Sun, R. Wang, C. M. Ko, Y. G. Ma, and C. Shen, Relativistic kinetic approach to light nuclei production in high-energy nuclear collisions, arXiv:2106.12742.

[29] A. Andronic, P. Braun-Munzinger, and J. Stachel, Hadron production in central nucleus-nucleus collisions at chemical freeze-out, Nucl. Phys. A **772**, 167 (2006).

[30] J. Cleymans, H. Oeschler, K. Redlich, and S. Wheaton, Comparison of chemical freeze-out criteria in heavy-ion collisions, Phys. Rev. C **73**, 034905 (2006).

[31] J. Adam *et al.* (STAR Collaboration), Beam energy dependence of (anti)deuteron production in Au+Au collisions at the BNL Relativistic Heavy Ion Collider, Phys. Rev. C **99**, 064905 (2019).

[32] STAR Collaboration, Beam energy dependence of triton production and yield ratio ($N_t \times N_p/N_d^2$) in Au+Au collisions at RHIC, arXiv:2209.08058.

[33] A. Andronic, P. Braun-Munzinger, J. Stachel, and H. Stocker, Production of light nuclei, hypernuclei and their antiparticles in relativistic nuclear collisions, Phys. Lett. B **697**, 203 (2011).

[34] V. Vovchenko, B. Dönigus, B. Kardan, M. Lorenz, and H. Stoecker, Feeddown contributions from unstable nuclei in relativistic heavy-ion collisions, Phys. Lett. B **809**, 135746 (2020).

[35] D. Zhang (STAR Collaboration), Light nuclei (d, t) production in Au+Au collisions at $\sqrt{s_{NN}} = 7.7$–200 GeV, Nucl. Phys. A **1005**, 121825 (2021); Energy dependence of light nuclei (d, t) production at STAR, JPS Conf. Proc. **32**, 010069 (2020).

[36] A. Andronic, P. Braun-Munzinger, K. Redlich, and J. Stachel, Decoding the phase structure of QCD via particle production at high energy, Nature (London) **561**, 321 (2018).

[37] S. Mrowczynski, Production of light nuclei at colliders—coalescence vs. thermal model, Eur. Phys. J. Spec. Top. **229**, 3559 (2020).

[38] M. Kozhevnikova, Y. B. Ivanov, I. Karpenko, D. Blaschke, and O. Rogachevsky, Update of the three-fluid hydrodynamics-based event simulator: Light-nuclei production in heavy-ion collisions, Phys. Rev. C **103**, 044905 (2021).

[39] Y. B. Ivanov, Baryon stopping as a probe of deconfinement onset in relativistic heavy-ion collisions, Phys. Lett. B **721**, 123 (2013).

[40] Y. B. Ivanov, Alternative scenarios of relativistic heavy-ion collisions: I. Baryon stopping, Phys. Rev. C **87**, 064904 (2013).

[41] Y. B. Ivanov, Alternative scenarios of relativistic heavy-ion

collisions: III. Transverse momentum spectra, Phys. Rev. C **89**, 024903 (2014).
[42] Y. B. Ivanov and A. A. Soldatov, Bulk properties of the matter produced at energies of the beam energy scan program, Phys. Rev. C **97**, 024908 (2018).
[43] T. Anticic *et al.* (NA49 Collaboration), Production of deuterium, tritium, and ^{3}He in central Pb+Pb collisions at 20*A*, 30*A*, 40*A*, 80*A*, and 158*A* GeV at the CERN Super Proton Synchrotron, Phys. Rev. C **94**, 044906 (2016).
[44] P. Batyuk, D. Blaschke, M. Bleicher, Y. B. Ivanov, I. Karpenko, S. Merts, M. Nahrgang, H. Petersen, and O. Rogachevsky, Event simulation based on three-fluid hydrodynamics for collisions at energies available at the Dubna Nuclotron-based Ion Collider Facility and at the Facility for Antiproton and Ion Research in Darmstadt, Phys. Rev. C **94**, 044917 (2016).
[45] P. Batyuk, D. Blaschke, M. Bleicher, Y. B. Ivanov, I. Karpenko, L. Malinina, S. Merts, M. Nahrgang, H. Petersen, and O. Rogachevsky, Three-fluid Hydrodynamics-based Event Simulator Extended by UrQMD final State interactions (THESEUS) for FAIR-NICA-SPSBES/RHIC energies, EPJ Web Conf. **182**, 02056 (2018).
[46] S. A. Bass, R. Mattiello, H. Stöcker, W. Greiner, and C. Hartnack, Is collective pion flow anticorrelated to nucleon flow? Phys. Lett. B **302**, 381 (1993).
[47] S. A. Bass *et al.*, Microscopic models for ultrarelativistic heavy ion collisions, Prog. Part. Nucl. Phys. **41**, 255 (1998).
[48] I. N. Mishustin, V. N. Russkikh, and L. M. Satarov, Fluid dynamical model of relativistic heavy ion collision, Sov. J. Nucl. Phys. **54**, 260 (1991).
[49] A. S. Khvorostukin, V. V. Skokov, V. D. Toneev, and K. Redlich, Lattice QCD constraints on the nuclear equation of state, Eur. Phys. J. C **48**, 531 (2006).
[50] Y. B. Ivanov, Alternative scenarios of relativistic heavy-ion collisions: II. Particle production, Phys. Rev. C **87**, 064905 (2013).
[51] Y. B. Ivanov and A. A. Soldatov, Light fragment production at CERN Super Proton Synchrotron, Eur. Phys. J. A **53**, 218 (2017).
[52] https://www.nndc.bnl.gov/nudat2/getdataset.jsp?nucleus=4HE&unc=nds.
[53] V. N. Russkikh and Yu. B. Ivanov, Dynamical freeze-out in three-fluid hydrodynamics, Phys. Rev. C **76**, 054907 (2007); Yu. B. Ivanov and V. N. Russkikh, On freeze-out problem in relativistic hydrodynamics, Phys. At. Nucl. **72**, 1238 (2009).
[54] H. Song, S. A. Bass, and U. Heinz, Viscous QCD matter in a hybrid hydrodynamic+Boltzmann approach, Phys. Rev. C **83**, 024912 (2011).
[55] M. Gazdzicki *et al.* (NA49 Collaboration), Report from NA49, J. Phys. G: Nucl. Part. Phys. **30**, S701 (2004).
[56] C. Alt *et al.* (NA49 Collaboration), High transverse momentum hadron spectra at $\sqrt{s_{NN}} = 17.3$ GeV in Pb + Pb and $p + p$ collisions, Phys. Rev. C **77**, 034906 (2008).
[57] T. Anticic *et al.* (NA49 Collaboration), Centrality dependence of proton and antiproton spectra in Pb+Pb collisions at 40*A* GeV and 158*A* GeV measured at the CERN SPS, Phys. Rev. C **83**, 014901 (2011).
[58] K. J. Sun, L. W. Chen, C. M. Ko, and Z. Xu, Probing QCD critical fluctuations from light nuclei production in relativistic heavy-ion collisions, Phys. Lett. B **774**, 103 (2017).
[59] K. J. Sun, L. W. Chen, C. M. Ko, J. Pu, and Z. Xu, Light nuclei production as a probe of the QCD phase diagram, Phys. Lett. B **781**, 499 (2018).
[60] X. Y. Zhao, Y. T. Feng, F. L. Shao, R. Q. Wang and J. Song, Production characteristics of light (anti-)nuclei from (anti-)nucleon coalescence in heavy ion collisions at energies employed at the RHIC beam energy scan, Phys. Rev. C **105**, 054908 (2022).
[61] Y. B. Ivanov and A. A. Soldatov, Directed flow indicates a cross-over deconfinement transition in relativistic nuclear collisions, Phys. Rev. C **91**, 024915 (2015); What can we learn from the directed flow in heavy-ion collisions at BES RHIC energies? Eur. Phys. J. A **52**, 10 (2016).
[62] J. Adam *et al.* (STAR Collaboration), Beam-energy dependence of the directed flow of deuterons in Au+Au collisions, Phys. Rev. C **102**, 044906 (2020).
[63] L. Adamczyk *et al.* (STAR Collaboration), Beam-Energy Dependence of the Directed Flow of Protons, Antiprotons, and Pions in Au+Au Collisions, Phys. Rev. Lett. **112**, 162301 (2014).
[64] N. U. Bastian, P. Batyuk, D. Blaschke, P. Danielewicz, Y. B. Ivanov, I. Karpenko, G. Röpke, O. Rogachevsky, and H. H. Wolter, Light cluster production at NICA, Eur. Phys. J. A **52**, 244 (2016).
[65] G. Röpke, D. Blaschke, Y. B. Ivanov, I. Karpenko, O. V. Rogachevsky, and H. H. Wolter, Medium effects on freeze-out of light clusters at NICA energies, Phys. Part. Nucl. Lett. **15**, 225 (2018).
[66] B. Dönigus, G. Röpke, and D. Blaschke, Deuteron yields from heavy-ion collisions at energies available at the CERN Large Hadron Collider: Continuum correlations and in-medium effects, Phys. Rev. C **106**, 044908 (2022).